# Chapter 4 Symmetry and Chemical Bonding

| |
|---|
| 4.1 Orbital Symmetries and Overlap |
| 4.2 Valence Bond Theory and Hybrid Orbitals |
| 4.3 Localized and Delocalized Molecular Orbitals |
| 4.4 $MX_n$ Molecules with Pi-Bonding |
| 4.5 Pi-Bonding in Aromatic Ring Systems |

# 4.1 Orbital Symmetries and Overlap

Bonded state can be represented by a Schrödinger wave equation of the general form

$$\mathcal{H}\Psi = E\Psi \qquad (4.1)$$

H; hamiltonian operator
Ψ; eigenfunction
E; eigenvalue

$$\mathcal{H} = -\sum_i \frac{h^2}{8\pi^2 m_i}\left(\frac{\partial^2}{\partial x_i^2} + \frac{\partial^2}{\partial y_i^2} + \frac{\partial^2}{\partial z_i^2}\right) + V(x_i, y_i, z_i) \qquad (4.2)$$

It is customary to construct approximate wave functions for the molecule from the atomic orbitals of the interacting atoms.

By this approach, when two atomic orbitals overlap in such a way that their individual wave functions add constructively, the result is a buildup of electron density in the region around the two nuclei.

# 4.1 Orbital Symmetries and Overlap

The association between the probability, *P*, of finding the electron at a point in space and the product of its wave function and its complex conjugate.

$$P \propto \Psi\Psi^* \qquad (4.3)$$

It the probability of finding it over all points throughout space is unity.

$$\int \Psi\Psi^* \, d\tau = 1 \qquad (4.4)$$

$$\int (N\psi)(N\psi^*) \, d\tau = N^2 \int \psi\psi^* \, d\tau = 1 \qquad (4.5)$$

N; normalization constant

# 4.1 Orbital Symmetries and Overlap

**Slater overlap integral**; the nature and effectiveness of their interactions

$$S = \int \Psi_A \Psi_B \, d\tau \qquad (4.6)$$

S>0, bonding interaction, a reinforcement of the total wave function and a buildup of electron density around the two nuclei
S<0, antibonding interaction, decrease of electron density in the region around the two nuclei
S=0, nonbonding interaction, electron density is essentially the same as before

# 4.1 Orbital Symmetries and Overlap

**Ballon representations**: these are rough representations of 90-99% of the probability distribution, which as the product of the wave function and its complex conjugate (or simply the square, if the function is real).

These are representations for the simplest examples of each type of orbital.

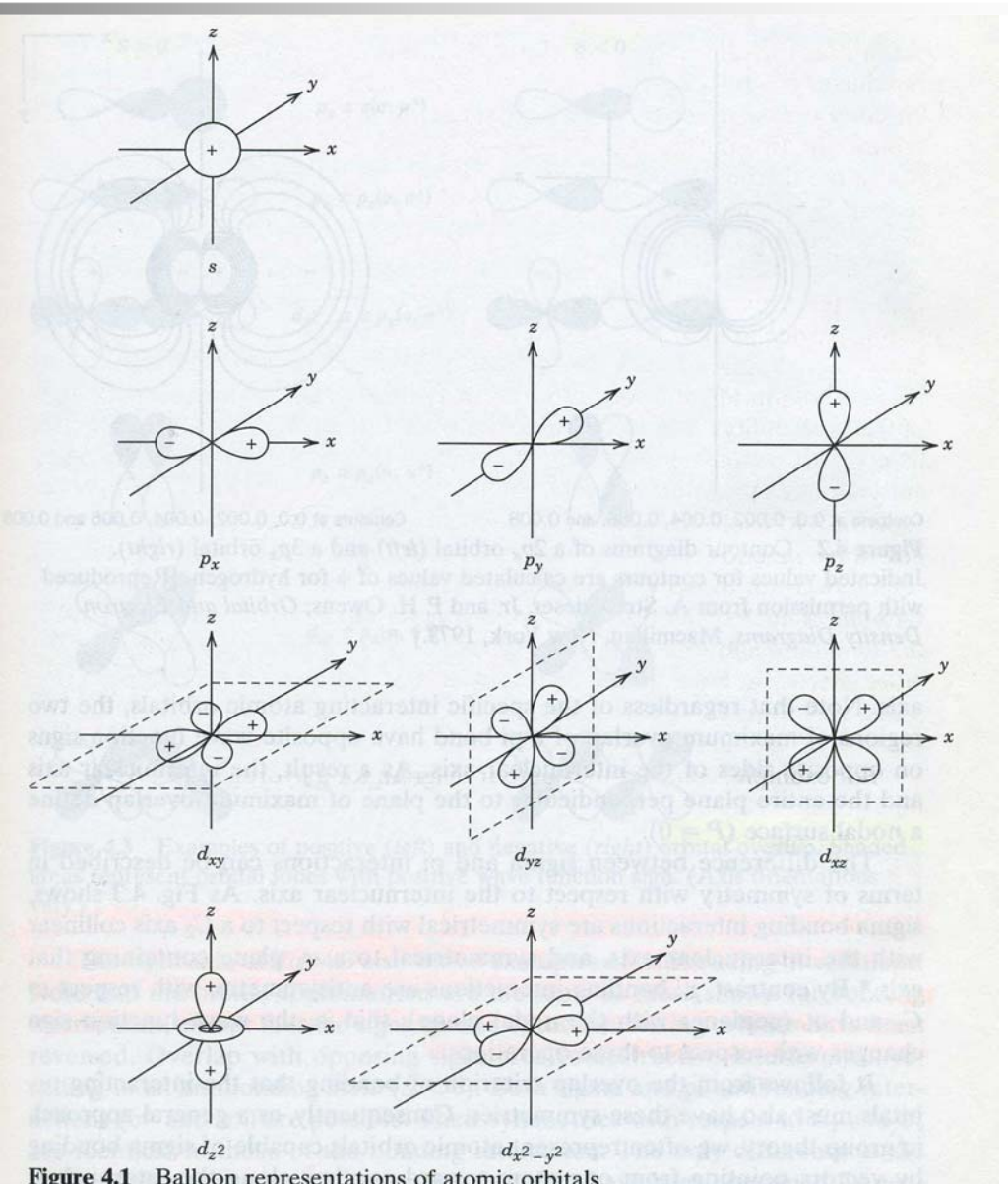



**Figure 4.1** Balloon representations of atomic orbitals

# 4.1 Orbital Symmetries and Overlap

Orbitals of each type with higher than the minimum allowed value of the principal quantum number *n* **have more nodes, and more lobes *but the symmetries of orbitals of the same type are identical***.

Symmetry of orbitals;
**$C_{\infty v}$ p orbitals**
**$D_{2h}$ $d_{xy}$ etc. orbitals**
**$D_{\infty h}$ $d_{z2}$ orbitals**

Therefore, for the purpose of analyzing symmetry aspects of orbital interaction and bonding, we usually may use the simplest example of an given type.

$2p_x$ $3p_x$

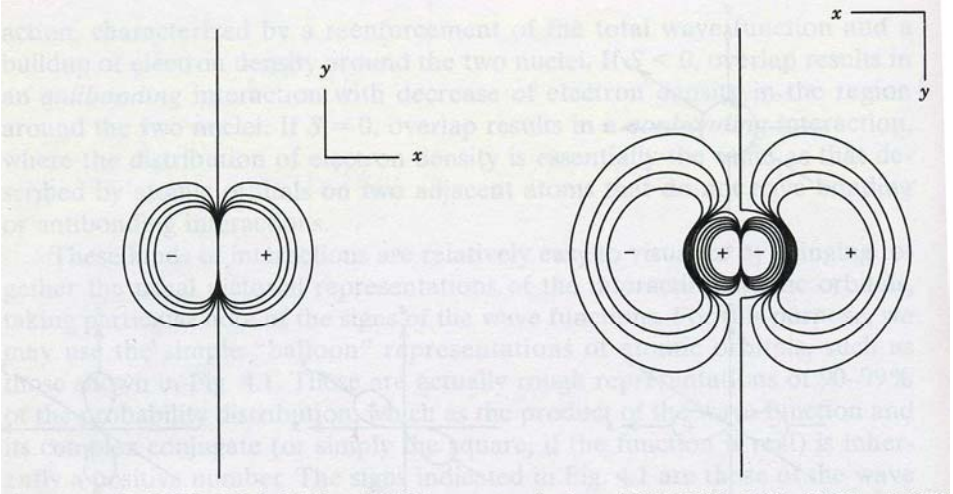



**Figure 4.2** Contour diagrams of a $2p_x$ orbital (*left*) and a $3p_x$ orbital (*right*). Indicated values for contours are calculated values of ψ for hydrogen. [Reproduced with permission from A. Streitwieser, Jr. and P. H. Owens, *Orbital and Electron Density Diagrams*, Macmillan, New York, 1973.]

# 4.1 Orbital Symmetries and Overlap

**Sigma bonding**
Reinforcement along the internuclear axis
The interacting orbitals need not be the same type

**Pi bonding**
Reinforcement above and below the internuclear axis
Nodal surface

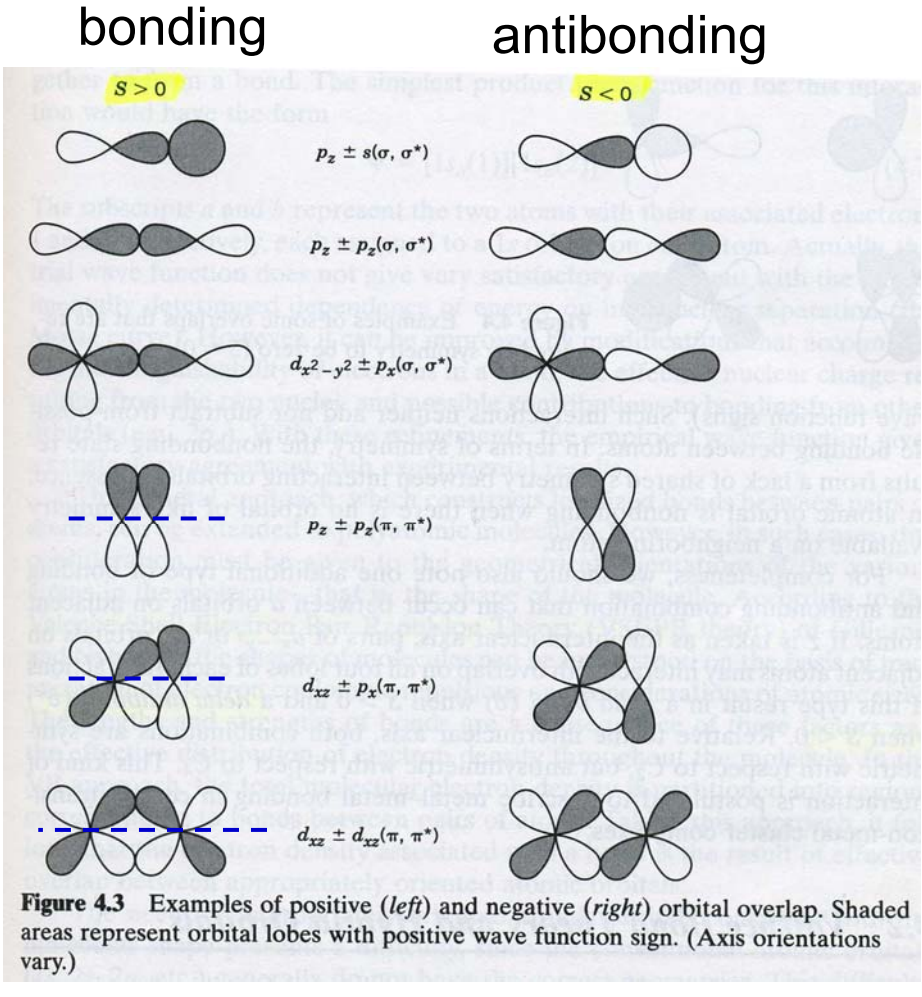


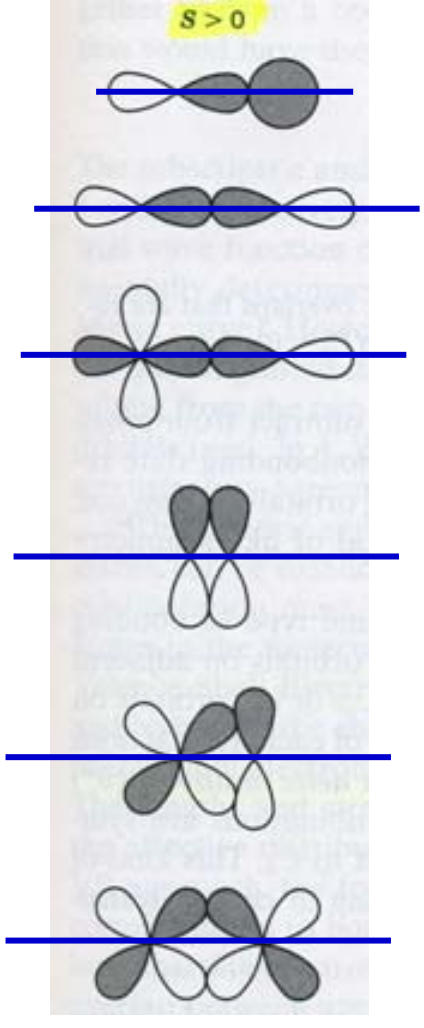

**Figure 4.3** Examples of positive (*left*) and negative (*right*) orbital overlap. Shaded areas represent orbital lobes with positive wave function sign. (Axis orientations vary.)

# 4.1 Orbital Symmetries and Overlap

The difference between sigma and pi interactions can be described ***in terms of symmetry with respect to the internuclear axis***.

Sigma bonding interactions are symmetrical with respect to a $C_2$ axis collinear with the internuclear axis, and symmetrical to a $\sigma_v$ plane containing that axis.

Pi bonding interactions are antisymmetric with respect to $C_2$ and $\sigma_v$.



# 4.1 Orbital Symmetries and Overlap

Nonbonding interactions; any region of reinforcement is counterbalanced by an equal region of destructive interference.

In terms of symmetry, the nonbonding state **results from a lack of shared symmetry between interacting orbitals**.

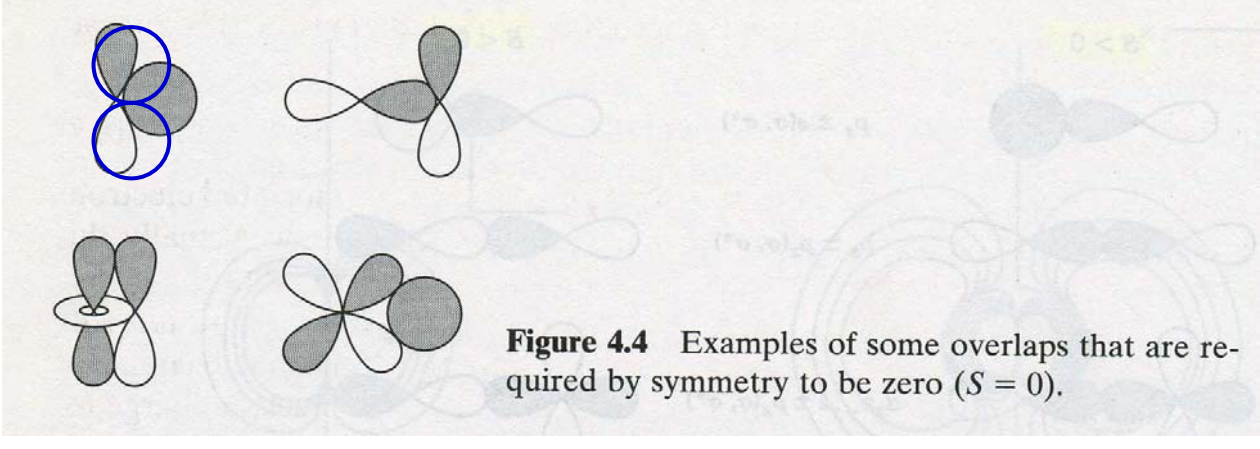


**Figure 4.4** Examples of some overlaps that are required by symmetry to be zero ($S = 0$).

**Delta bond** (pairs of $d_{x2-y2}$ or $d_{xy}$); interact with overlap on all four lobes of each.
Metal-metal bonding

# 4.2 Valence Bond Theory and Hybrid Orbitals

Valence bond Theory; it is an extension of the Lewis idea of bond formation through sharing of electron pairs.

In the VB approach, the electron density between bonding atoms can be defined on the basis of a new wave function, which in its simplest formulation is a product of the wave functions of the interacting orbitals.

For two hydrogen atom:

$$\Psi = [1s_a(1)][1s_b(2)] \qquad (4.7)$$

# 4.2 Valence Bond Theory and Hybrid Orbitals

This general approach, which constructs localized bonds between pairs of atoms, can be extended to polyatomic molecules.

However, we must consider **the geometrical orientations**

According to the Valence Shell Electron Pair Repulsion Theory (VSEPR), the shapes of molecules can be understood on the basis of **minimization of electron coulombic repulsions and considerations of atomic sizes**.

The electron density associated with a bond is **the result of effective overlap between appropriately oriented atomic orbitals**.

# 4.2 Valence Bond Theory and Hybrid Orbitals

The need for appropriately oriented atomic orbitals consistent with the molecular shape presents a difficulty, since the conventional atomic orbitals generally do not have the correct geometries.

The formation of hybrid orbitals consistent with the geometrical requirements of molecules.

$^3P$ ground state carbon change to $^5S$ state.
Additional energy would be required to create four tetrahedrally directed hybrid orbitals ($V_4$)

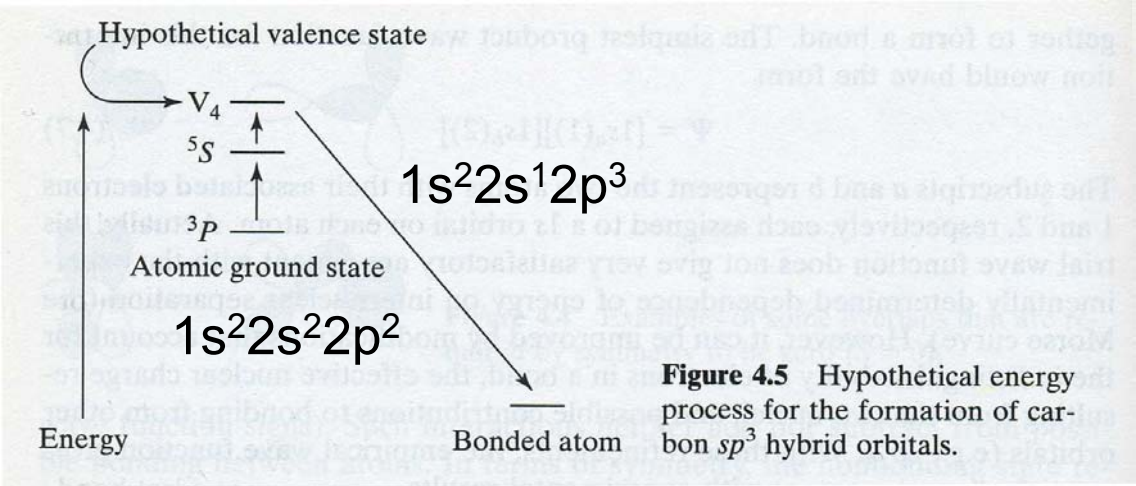



**Figure 4.5** Hypothetical energy process for the formation of carbon $sp^3$ hybrid orbitals.

# 4.2 Valence Bond Theory and Hybrid Orbitals

This hypothetical process is merely a convenient artifice.

In the case of tetrahedrally bonded carbon, combination of *2s, 2p*$_x$, *2p*$_y$, *2p*$_z$ lead to the following four wave functions:

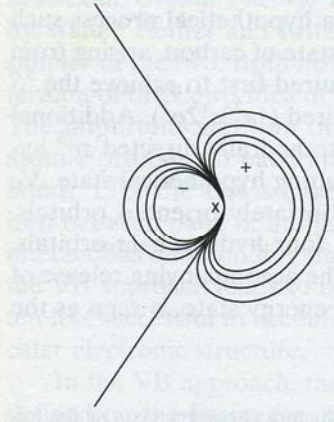
$$\Psi_1 = \frac{1}{2}(s + p_x + p_y + p_z) \quad (4.8a)$$

$$\Psi_2 = \frac{1}{2}(s + p_x - p_y - p_z) \quad (4.8b)$$

$$\Psi_3 = \frac{1}{2}(s - p_x + p_y - p_z) \quad (4.8c)$$

$$\Psi_4 = \frac{1}{2}(s - p_x - p_y + p_z) \quad (4.8d)$$

Each resulting orbital has the same shape and is oriented at 109.28º from any other orbital of the set.




Contours at 0.0, 0.002, 0.004, 0.006, and 0.008

**Figure 4.6** Contour diagram of a single $sp^3$ hybrid orbital. The two straight lines indicate the two-dimensional projection of a conical node. Indicated values for contours are calculated values of ψ. [Reproduced with permission from A. Streitwieser, Jr. and P. H. Owens, *Orbital and Electron Density Diagrams*, Macmillan, New York, 1973.]

# 4.2 Valence Bond Theory and Hybrid Orbitals

The $sp^3$ combination of standard atomic orbitals is not the only one that can be involved in tetrahedral bonding.

We must recognize the ways in which the standard atomic orbitals will transform in any point group.

In any molecular point group an *s* orbital at the center of the system will transform as the totally symmetric representation.

The orientation of the three *p* orbitals along the cardinal axes of the coordinate system allows them to be represented by a unit vector along the same axis. Noted in the next-to-last column of each character table.

The *d* orbitals are listed in the last column of each character table.

# 4.2 Valence Bond Theory and Hybrid Orbitals

We will presume that a set of four tetrahedrally directed hybrid orbitals can be formed, and we will make it the basis for a representation in the point group of a tetrahedron, $T_d$.

If we subject this basis set to the operations of $T_d$, we can **deduce the characters of a reducible representation ($\Gamma_t$).**

**Finally, reducing** the representation $\Gamma_t$ into its component irreducible representations will enable us to identify conventional orbitals with the required symmetries to form a tetrahedral set of hybrids.

# 4.2 Valence Bond Theory and Hybrid Orbitals

Represent the four equivalent hybrid orbitals by vectors.

4 X 1 matrix to represent the positions before and after each operation.

The transformation effected by each operation will be represented by a 4 X 4 transformation matrix, whose trace will generate a character for the operation, which in turn will become part of our reducible representation $\Gamma_t$ in $T_d$.

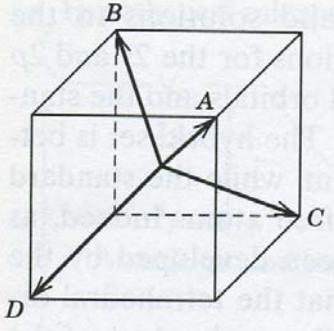
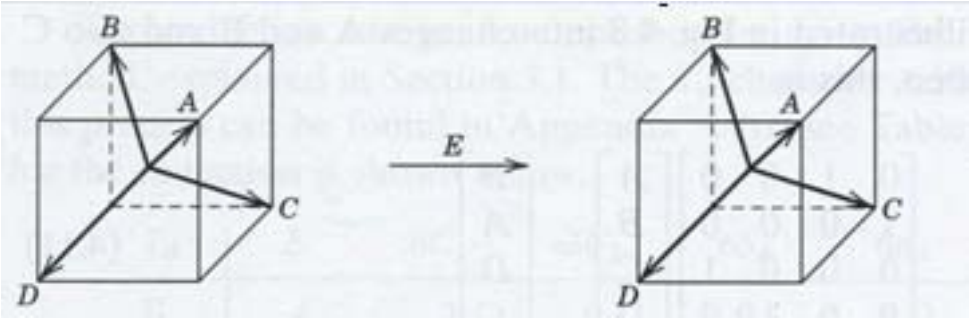



**Figure 4.7** Vector basis for a representation of tetrahedral orbitals in $T_d$.

# 4.2 Valence Bond Theory and Hybrid Orbitals

For the identity operation, E




4 X 4 transformation matrix

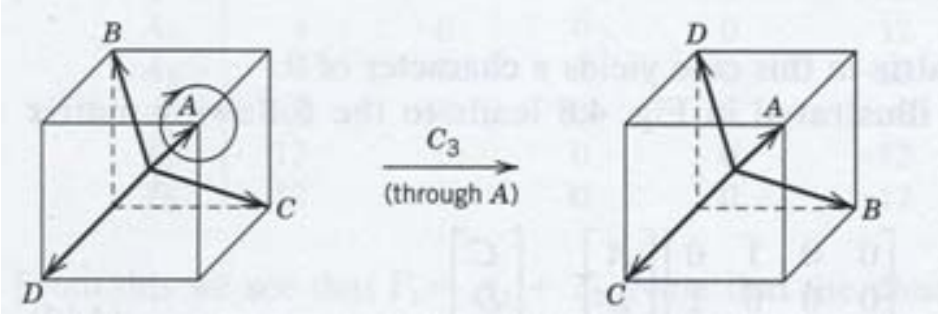
$$\begin{bmatrix} 1 & 0 & 0 & 0 \\ 0 & 1 & 0 & 0 \\ 0 & 0 & 1 & 0 \\ 0 & 0 & 0 & 1 \end{bmatrix} \begin{bmatrix} A \\ B \\ C \\ D \end{bmatrix} = \begin{bmatrix} A \\ B \\ C \\ D \end{bmatrix}$$

4 X 1 matrix to represent the positions before and after each operation.

The trace of the 4 X 4 transformation matrix gives a **character of 4**.

# 4.2 Valence Bond Theory and Hybrid Orbitals

For the $C_3$ operation

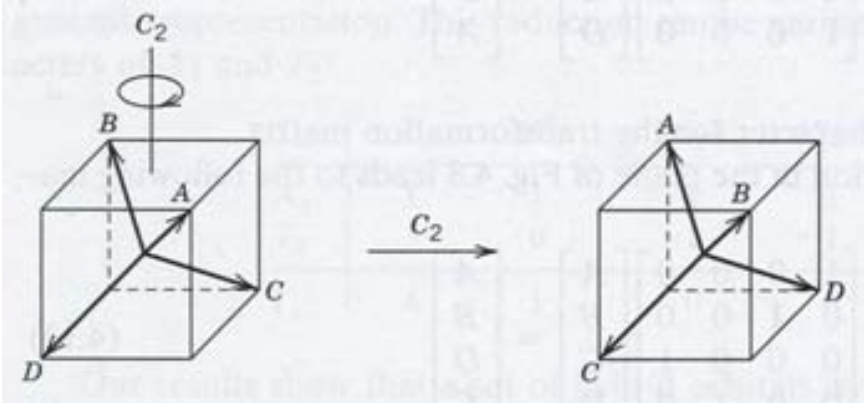



$$\begin{bmatrix} 1 & 0 & 0 & 0 \\ 0 & 0 & 0 & 1 \\ 0 & 1 & 0 & 0 \\ 0 & 0 & 1 & 0 \end{bmatrix} \begin{bmatrix} A \\ B \\ C \\ D \end{bmatrix} = \begin{bmatrix} A \\ D \\ B \\ C \end{bmatrix} \qquad (4.10)$$

The trace of the 4 X 4 transformation matrix gives a **character of 1**.

# 4.2 Valence Bond Theory and Hybrid Orbitals

For the $C_2$ operation

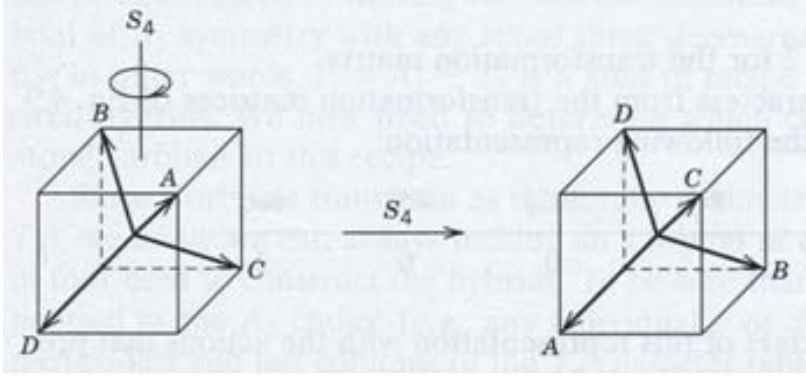



$$\begin{bmatrix} 0 & 1 & 0 & 0 \\ 1 & 0 & 0 & 0 \\ 0 & 0 & 0 & 1 \\ 0 & 0 & 1 & 0 \end{bmatrix} \begin{bmatrix} A \\ B \\ C \\ D \end{bmatrix} = \begin{bmatrix} B \\ A \\ D \\ C \end{bmatrix} \qquad (4.11)$$

The trace of the 4 X 4 transformation matrix gives a **character of 0**.

# 4.2 Valence Bond Theory and Hybrid Orbitals

For the $S_4$ operation

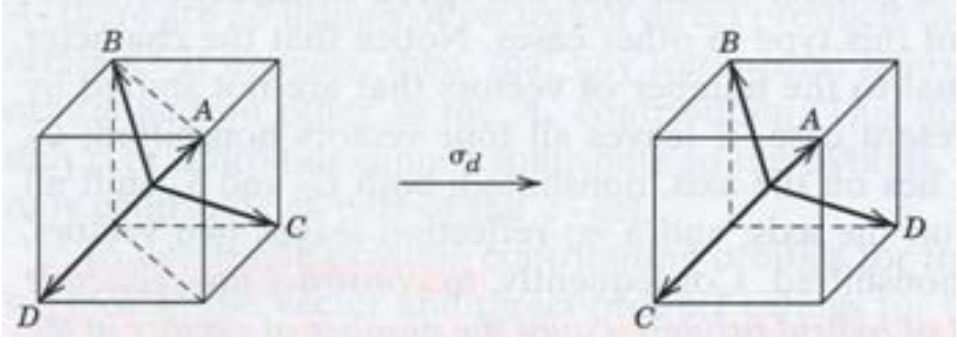



$$\begin{bmatrix} 0 & 0 & 1 & 0 \\ 0 & 0 & 0 & 1 \\ 0 & 1 & 0 & 0 \\ 1 & 0 & 0 & 0 \end{bmatrix} \begin{bmatrix} A \\ B \\ C \\ D \end{bmatrix} = \begin{bmatrix} C \\ D \\ B \\ A \end{bmatrix} \qquad (4.12)$$

The trace of the 4 X 4 transformation matrix gives a ***character of 0.***

# 4.2 Valence Bond Theory and Hybrid Orbitals

For the $\sigma_d$ operation




$$\begin{bmatrix} 1 & 0 & 0 & 0 \\ 0 & 1 & 0 & 0 \\ 0 & 0 & 0 & 1 \\ 0 & 0 & 1 & 0 \end{bmatrix} \begin{bmatrix} A \\ B \\ C \\ D \end{bmatrix} = \begin{bmatrix} A \\ B \\ D \\ C \end{bmatrix} \qquad (4.13)$$

The trace of the 4 X 4 transformation matrix gives a **character of 2**.

# 4.2 Valence Bond Theory and Hybrid Orbitals

Gathering all the characters from the transformation matrices, we obtain the following representation.

| $T_d$ | $E$ | $8C_3$ | $3C_2$ | $6S_4$ | $6\sigma_d$ |
|---|---|---|---|---|---|
| $\Gamma_t$ | 4 | 1 | 0 | 0 | 2 |

Notice that the **character for each operation** is equal to **the number of vectors that are not shifted by the operation**.

The number of nonshifted vectors is the character for the class in each case.

# 4.2 Valence Bond Theory and Hybrid Orbitals

Reduction can be accomplished by **using Eq. 3.1 and tabular method**.

| $T_d$ | $E$ | $8C_3$ | $3C_2$ | $6S_4$ | $6\sigma_d$ | | |
|---|---|---|---|---|---|---|---|
| $\Gamma_t$ | 4 | 1 | 0 | 0 | 2 | $\Sigma$ | $\Sigma/24$ |
| $A_1$ | 4 | 8 | 0 | 0 | 12 | 24 | 1 |
| $A_2$ | 4 | 8 | 0 | 0 | −12 | 0 | 0 |
| $E$ | 8 | −8 | 0 | 0 | 0 | 0 | 0 |
| $T_1$ | 12 | 0 | 0 | 0 | −12 | 0 | 0 |
| $T_2$ | 12 | 0 | 0 | 0 | 12 | 24 | 1 |

From this we see that $\Gamma_t = A_1 + T_2$.

| $T_d$ | $E$ | $8C_3$ | $3C_2$ | $6S_4$ | $6\sigma_d$ |
|---|---|---|---|---|---|
| $A_1$ | 1 | 1 | 1 | 1 | 1 |
| $T_2$ | 3 | 0 | −1 | −1 | 1 |
| $\Gamma_t$ | 4 | 1 | 0 | 0 | 2 |

# 4.2 Valence Bond Theory and Hybrid Orbitals

Our results show that a set of hybrid orbitals with tetrahedral geometry **can be constructed by making suitable mathematical combinations of any orbital of $A_1$ symmetry with any set of three degenerate orbitals of $T_2$ symmetry**.

In order word, $\Gamma_t = A_1 + T_2$ **is a kind of recipe** for constructing the desired hybrids.

We must determine which combinations of specific atomic orbitals fit this recipe.

*s* orbital is only atomic orbital as $A_1$ from character table.

So, any tetrahedral hybrid set must include an *s* orbital.

# 4.2 Valence Bond Theory and Hybrid Orbitals

Degenerate vectors (x, y, z), which in this context signify the three *p* orbitals.
Three degenerate direct products (xy, yz, xz), which signify a degenerate set of the three specific d orbitals.

Since there are two sets of orbitals with $T_2$ symmetry, there are two possible choice of triply degenerate orbitals to include in constructing a hybrid set.

We can construct two sets of hybrid, ***sp*$^3$ and *sd*$^3$ hybrids**.

Which hybrid set is correct?- the answer depends upon the energies of *d* orbitals for the central atom.

For example, in carbon the energy of the *d* orbitals lies so much higher than that of the *p* orbitals, so $sp^3$ hybrids.

In transition metal, *d* orbital participation may be significant.

# 4.2 Valence Bond Theory and Hybrid Orbitals

Note that the $d_{x2-y2}$ and $d_{z2}$ orbitals cannot contribute to forming a tetrahedral set of hybrid orbitals.

The number of atomic orbitals used is same with the number of hybrid orbitals formed.

This approach can be used to deduce appropriate AO combinations for hybrids consistent with the other primary shapes predicted by VSEPR theory.

# 4.2 Valence Bond Theory and Hybrid Orbitals

For another example, ***$D_{\infty h}$*** **($CO_2$).**

1. Represent the two equivalent hybrid orbitals by vectors.

2. 2 X 1 matrix to represent the positions before and after each operation.

3. The transformation effected by each operation will be represented by a 2 X 2 transformation matrix, whose trace will generate a character for the operation, which in turn will become part of our reducible representation $\Gamma_I$ in $D_{\infty h}$.



# 4.2 Valence Bond Theory and Hybrid Orbitals

The number of nonshifted vectors is the character for the class in each case.




| $D_{\infty h}$ | $E$ | $2C_\infty^\Phi$ | … | $\infty\sigma_v$ | $i$ | $2S_\infty^\Phi$ | … | $\infty C_2$ |
|---|---|---|---|---|---|---|---|---|
| $\Gamma_l$ | 2 | 2 | … | 2 | 0 | 0 | … | 0 |

By inspection of character table, we can see that this decomposes as the following two irreducible representation.

| $D_{\infty h}$ | $E$ | $2C_\infty^\Phi$ | … | $\infty\sigma_v$ | $i$ | $2S_\infty^\Phi$ | … | $\infty C_2$ |
|---|---|---|---|---|---|---|---|---|
| $\Sigma_g^+$ | 1 | 1 | … | 1 | 1 | 1 | … | 1 |
| $\Sigma_u^+$ | 1 | 1 | … | 1 | −1 | −1 | … | −1 |
| $\Gamma_l$ | 2 | 2 | … | 2 | 0 | 0 | … | 0 |

This results means that we can construct a set of linear hybrid orbitals by taking combinations of one orbital of $\Sigma_g^+$ symmetry with one orbital of $\Sigma_u^+$ symmetry.

# 4.2 Valence Bond Theory and Hybrid Orbitals

By inspection of the character table

*s* and $d_{z2}$ orbitals can use as part of a hybrid set. $\Sigma_g^+$

$p_z$ orbital can use as other part of a hybrid set. $\Sigma_u^+$

We can construct two sets of hybrid, *sp* and *dp* hybrids.

Using the *sp* set as a model, the hybrid orbital wave functions have the following form

$$\Psi_1 = \frac{1}{\sqrt{2}}(s + p_z) \qquad (4.14a)$$

$$\Psi_2 = \frac{1}{\sqrt{2}}(s - p_z) \qquad (4.14b)$$

# 4.3 Localized and Delocalized Molecular Orbitals

In the VB approach the interacting orbitals in a chemical bond may be viewed as retaining much of their atomic character.

By contrast, the molecular orbital approach seeks to construct new wave functions that define unique orbitals for the bonded system.

In principle, the task amounts to defining the Schrödinger wave equation for a system in which the nuclei of the individual atoms are treated as if they formed a polycentric nucleus embedded in an electron distribution that **surrounds the entire molecule**.

If the relative energies of these MOs are known, the ground-state configuration of the molecule can **be deduced by an aufbau process**, much like that used for determining the ground state configurations of single atoms.

As with the case of isolated atoms, the aufbau process obeys the Pauli Exclusion Principle and Hund's Rule of Maximum Multiplicity.

# 4.3 Localized and Delocalized Molecular Orbitals

In practice, the exact construction and solution of a molecular wave equation is not feasible except in the simplest diatomic cases.

Therefore, it is customary to construct empirical wave functions as mathematical sums of wave functions on the various atoms of the molecule.

This approach is called the **Linear Combination of Atomic Orbitals (LCAO) method**.

In the case of a general diatomic molecule, AB, wave functions for the molecule take on the forms in which *a* and *b* are constants, sometimes called mixing constant, that reflect the **relative contributions** of each wave function to the LCAO wave function.

$$\Psi_1 = a\psi + b\psi \qquad (4.15a)$$

$$\Psi_2 = a\psi - b\psi \qquad (4.15b)$$

# 4.3 Localized and Delocalized Molecular Orbitals

Atomic orbitals used to construct these MOs (1) must have similar energies, (2) must overlap appreciably, and (3) must have the same symmetry with respect to the internuclear axis.

If Eq. 4.15a results in reinforcement ($S > 0$), the resulting LCAO will define a bonding MO.
Eq. 4.15b defines an antibonding MO ($S < 0$).

The antibonding MO always has a higher energy than the corresponding bonding MO.

Assuming hybridization on the central atom, *a priori*, is most often useful when taking a localized MO approach.

The LCAO wave functions in this limited approach **involve only two atoms** and take on forms such as Eq 4.15.

# 4.3 Localized and Delocalized Molecular Orbitals

The Lewis model for gaseous $BeH_2$ is simply H-Be-H, from which VSEPR theory predicts a linear structure ($D_{\infty h}$).

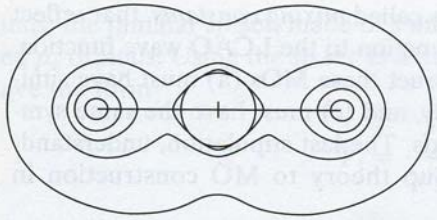



**Figure 4.9** Electron density about $BeH_2$. Indicated values for contours are calculated values of $\psi$. [Reproduced with permission from A. Streitwieser, Jr. and P. H. Owens, *Orbital and Electron Density Diagrams*, Macmillan, New York, 1973.]

The VB approach implicitly partitions this distribution into two equivalent Be-H bonds, each formed by overlap of one sp hybrid orbital on the beryllium atom with a 1s orbital on a hydrogen atom.

We can extend this model to become a localized MO model by defining wave functions between pairs of adjacent atoms with the following forms.

$$\sigma_1 = a[sp(1)_{Be}] + b[1s_{H'}] \quad (4.16a)$$

$$\sigma_2 = a[sp(2)_{Be}] + b[1s_{H''}] \quad (4.16b)$$

$$\sigma_3^* = a[sp(1)_{Be}] - b[1s_{H'}] \quad (4.16c)$$

$$\sigma_4^* = a[sp(2)_{Be}] - b[1s_{H''}] \quad (4.16d)$$

# 4.3 Localized and Delocalized Molecular Orbitals

There are two bonding MOs and two antibonding MOs.

We can construct a qualitative molecular orbital energy level diagram.

The filling of electrons in the MOs follows in an aufbau manner.

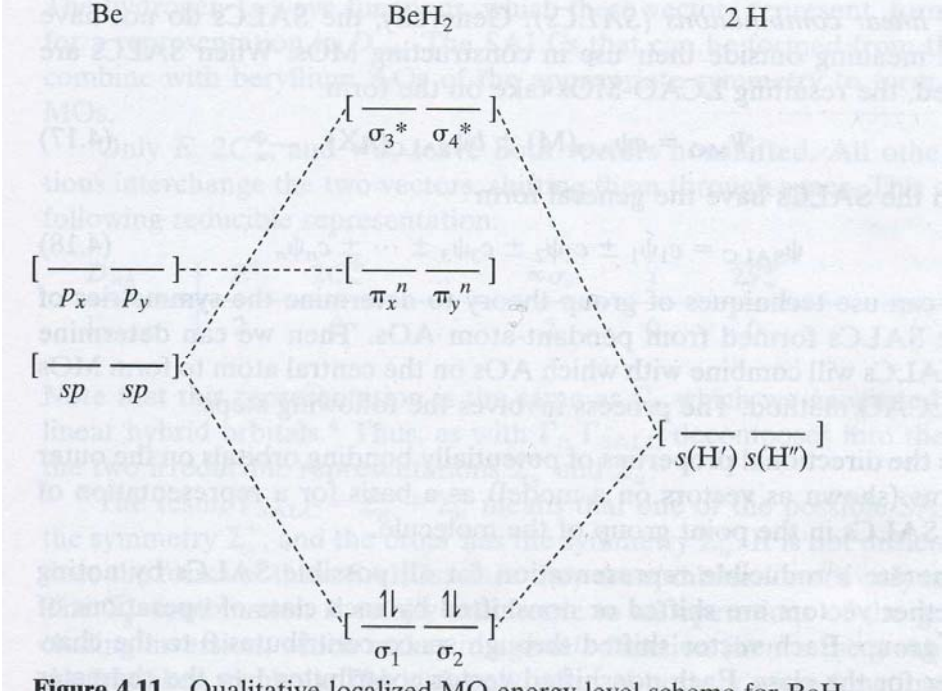



**Figure 4.11** Qualitative localized MO energy level scheme for $BeH_2$.

# 4.3 Localized and Delocalized Molecular Orbitals

The localized MO scheme for $BeH_2$ suggests that two pairs of electrons are localized in degenerate bonding MOs.

This is, however, somewhat misleading.

The equivalence of the bonding sigma MOs is artificial, since in setting up the problem we constrained the electrons to be localized in two equivalent regions.

Nonetheless, such localized MO models are useful for discussions of chemical bonds and accounting for bonding and nonbonding electron pairs.

# 4.3 Localized and Delocalized Molecular Orbitals

If we do not constrain electrons to localized bonds, **we will obtain a general or delocalized MO model**.

This approach usually yields MOs with energies that are more consistent with electronic spectra and ionization energies.

However, this approach requires that we abandon the VB notion of a chemical bond as the sharing of a pair of electrons by two adjacent atoms.

In the general MO approach, MOs and the electrons associated with them **typically extend across the molecule**.

# 4.3 Localized and Delocalized Molecular Orbitals

For simple molecules of the type $MX_n$ we can approach the problem **by matching symmetries of the orbitals** on the central M atom with those of mathematical combinations of orbitals on the outer X atoms, called pendant atoms.

These mathematical constructs of pendent-atom AOs are called **symmetry-adapted linear combinations (SALCs).**

When SALCs are employed, the resulting LCAO-MOs take on the from

$$\Psi_{MO} = a\psi_{AO}(M) \pm b\psi_{SALC}(nX) \quad (4.17)$$

in which the SALCs have the general form

$$\psi_{SALC} = c_1\psi_1 \pm c_2\psi_2 \pm c_3\psi_3 \pm \cdots \pm c_n\psi_n \quad (4.18)$$

# 4.3 Localized and Delocalized Molecular Orbitals

We can use **techniques of group theory to determine the symmetries of possible SALCs formed from pendant-atom AOs**.

Then we can determine which SALCs will combine with which AOs on the central atoms to from MOs by LCAO method.

# 4.3 Localized and Delocalized Molecular Orbitals

Generate the general MO model for $BeH_2$.

The two hydrogen *1s* orbitals can only form sigma interactions, so we will represent them as two vectors pointing towards the central beryllium atom.

The SALCs that can be formed from hydrogen will combine with beryllium AOs of the appropriate symmetry to form LCAO-MOs.



| $D_{\infty h}$ | $E$ | $2C_{\infty}^{\Phi}$ | … | $\infty\sigma_v$ | $i$ | $2S_{\infty}^{\Phi}$ | … | $\infty C_2$ |
|---|---|---|---|---|---|---|---|---|
| $\Gamma_{SALC}$ | 2 | 2 | … | 2 | 0 | 0 | … | 0 |

$\Gamma_{SALC}$ decomposes into the sum of the two irreducible representations. $\Sigma_g^+$ $\Sigma_u^+$

# 4.3 Localized and Delocalized Molecular Orbitals

The result means that one of the possible SALCs has the symmetry $\Sigma_g^+$, and the other has the symmetry $\Sigma_u^+$.

The $\Sigma_g^+$ combination is totally symmetric to all operations of the group, including inversion, which makes if a ***gerade*** function.

This can occur if both *1s* wave function on the two hydrogen atoms are combined in a positive sense.

The $\Sigma_u^+$ combination is ***ungerade***, which implies a change of sign with the operation of inversion.

This would occur if one *1s* wave function were taken in the positive sense and the other were taken in the negative sense

# 4.3 Localized and Delocalized Molecular Orbitals

The two normalized SALCs must have the following form.

$$\Phi_g = \frac{1}{\sqrt{2}}(1s_{H'} + 1s_{H''}) \qquad (4.19a)$$

$$\Phi_u = \frac{1}{\sqrt{2}}(1s_{H'} - 1s_{H''}) \qquad (4.19b)$$

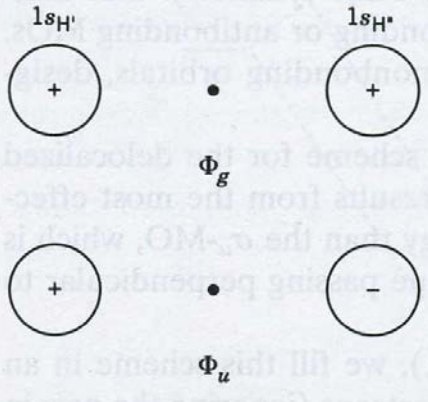



**Figure 4.12** Symmetry-adapted linear combinations (SALCs) of hydrogen 1*s* orbitals for $BeH_2$.

# 4.3 Localized and Delocalized Molecular Orbitals

In order for the SALCs to form bonding and antibonding combinations, AOs with the same symmetry properties must exist on the beryllium atom.

The *s* orbitals of the central atom transform as the totally symmetric representation, here $\Sigma_g^+$.
From character table, we see that $p_z$ transforms as $\Sigma_u^+$ and that $p_x$ and $p_y$ transform as degenerate pair by $\Pi_u$.

The symmetry of the 2*s* orbital on the beryllium atom matches that of the SALC $\Phi_g$ of two hydrogen atoms.

We can form bonding and antibonding MOs with the following wave function.

$$\sigma_g = c_1 2s + c_2 \Phi_g \qquad (4.20a)$$

$$\sigma_g^* = c_3 2s - c_4 \Phi_g \qquad (4.20b)$$

# 4.3 Localized and Delocalized Molecular Orbitals

In similar manner, the $2p_z$ orbital matches the $\Sigma_u^+$ symmetry of the $\Phi_u$ SALC, giving MOs with the following wave function

$$\sigma_u = c_5 2p_z + c_6 \Phi_u \qquad (4.20c)$$

$$\sigma_u^* = c_7 2p_z - c_8 \Phi_u \qquad (4.20d)$$

# 4.3 Localized and Delocalized Molecular Orbitals

Note that these orbitals extend across the entire molecule and are not confined to individual bonds.

Nontheless, the bonding MOs are characterized by reinforcement in the region of each Be-H bond, while the antibonding MOs are characterized by a nodal plane passing between each Be-H pair.

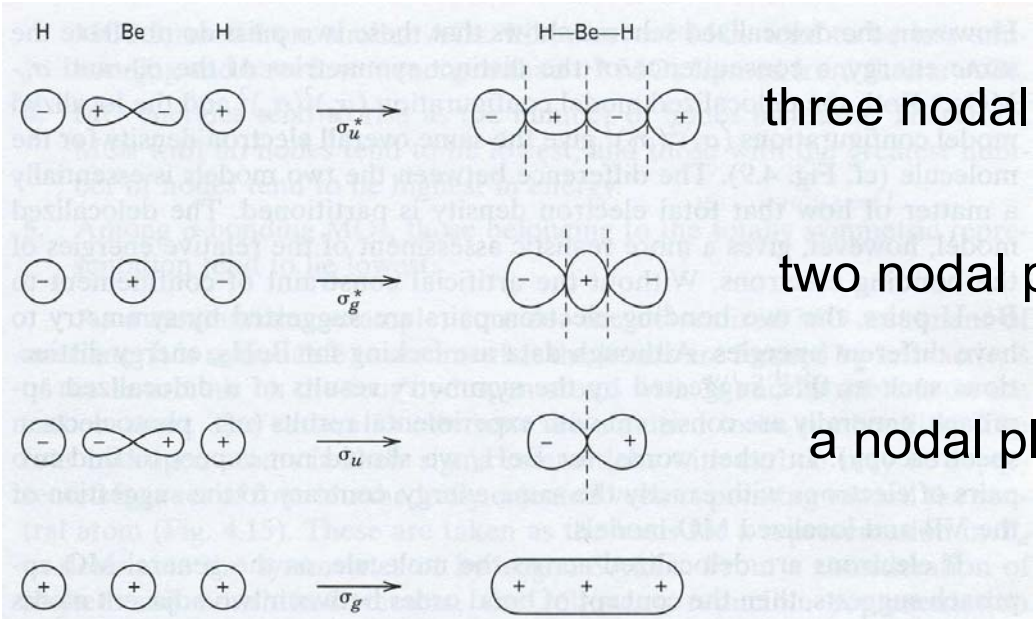



**Figure 4.13** Linear combinations of atomic orbitals (LCAOs) and the resulting delocalized bonding ($\sigma_g$ and $\sigma_u$) and antibonding ($\sigma_g^*$ and $\sigma_u^*$) molecular orbitals (MOs) of $BeH_2$. Dashed lines indicate nodal planes perpendicular to the molecular axis. Orbital energy increases from bottom to top.

# 4.3 Localized and Delocalized Molecular Orbitals

The $2p_x$ and $2p_y$ orbitals on beryllium have no matching SALCs with the same symmetry-nonbonding orbitals..

delocalized MOs

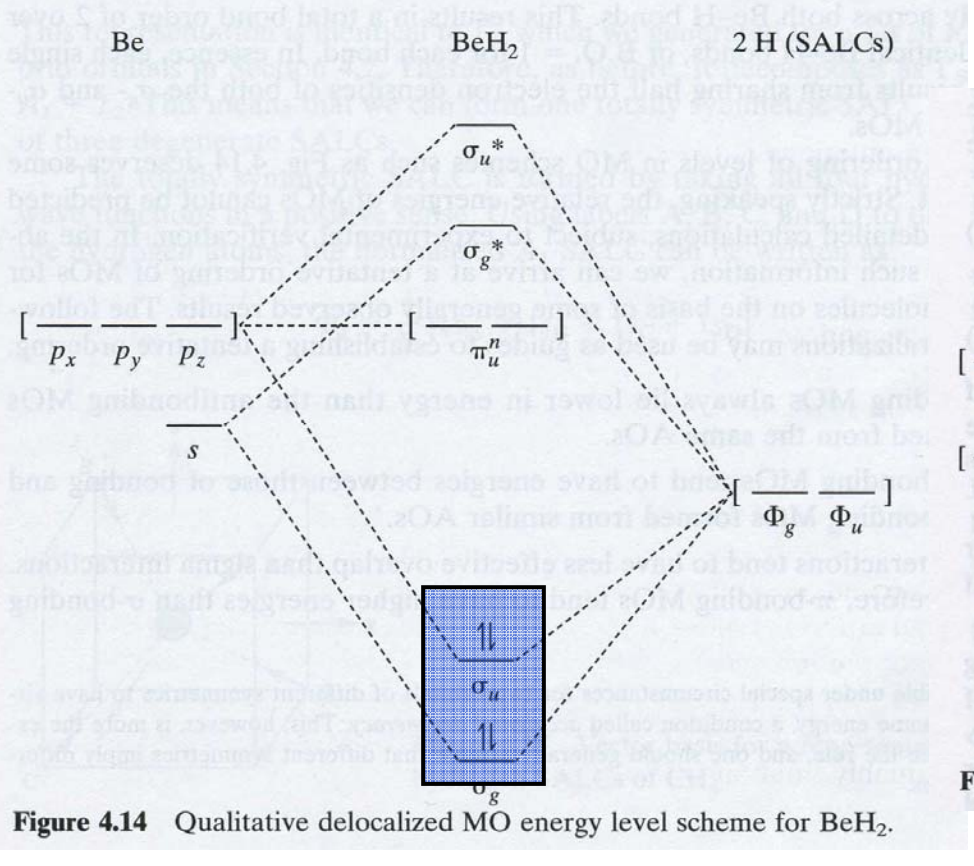



**Figure 4.14** Qualitative delocalized MO energy level scheme for $BeH_2$.

localized MOs

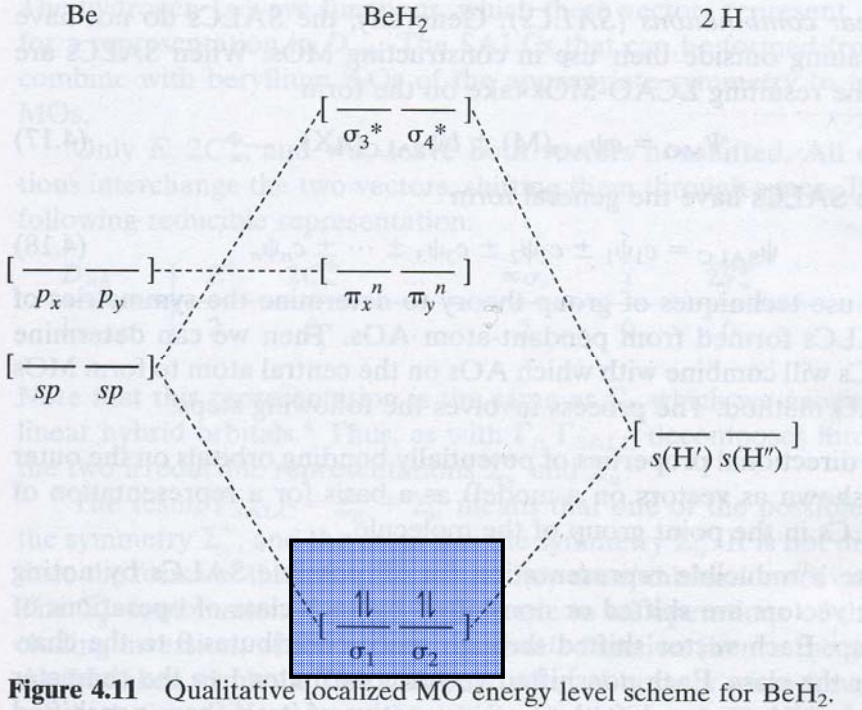



**Figure 4.11** Qualitative localized MO energy level scheme for $BeH_2$.

# 4.3 Localized and Delocalized Molecular Orbitals

The difference between the two model is essentially a matter of how that total electron density is partitioned.

Without the artificial constraint of confinement to Be-H pairs, the two bonding electron pairs are suggested by symmetry to have different energies.

The symmetry results of a delocalized approach are consistent with experimental results.

In other words, for $BeH_2$ we should not expect to find two pairs of electrons with exactly the same energy, contrary to the suggestion of the VB and localized MO models.

Each single bond results from sharing half the electron densities of both the $\sigma_{g-}$ and $\sigma_{u-}$ bonding MOs.

# 4.3 Localized and Delocalized Molecular Orbitals

The ordering of levels in MO schemes.

Strictly speaking, the relative energies of MOs cannot be predicted without detailed calculations, subject to experimental verification.

The following generalizations may be used as guides to establishing a tentative ordering.

1. Bonding MOs always lie lower in energy than the antibonding MOs formed from the same AOs.
2. Nonbonding MOs tend to have energies between those of bonding and antibonding MOs formed from similar AOs.
3. Pi interactions tend to have less effective overlap than sigma interactions. Therefore, $\pi$-bonding MOs tend to have higher energies than $\sigma$-bonding MOs formed from similar AOs. Likewise, $\pi^*$ MOs tend to be less antibonding and have lower energies than $\sigma^*$ MOs formed from similar AOs.
4. MO energies tend to rise as the number of nodes increases. Therefore, MOs with no nodes tend to lie lowest, and those with the greatest number of nodes tend to lie highest in energy.
5. Among $\sigma$-bonding MOs, those belonging to the totally symmetric representation tend to lie lowest.

# 4.3 Localized and Delocalized Molecular Orbitals

Another example **$CH_4$**.

The four hydrogen atoms in their sigma interactions with carbon may be represented by a set of four tetrahedrally oriented vectors pointing toward the central atom.

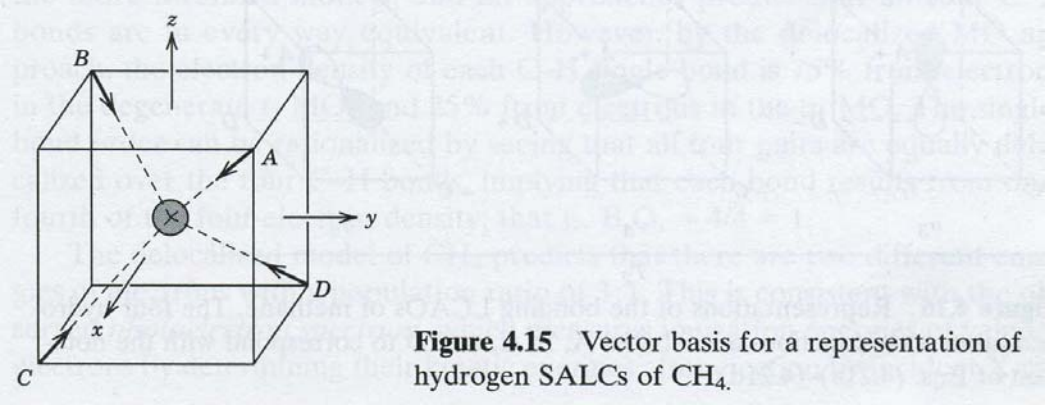
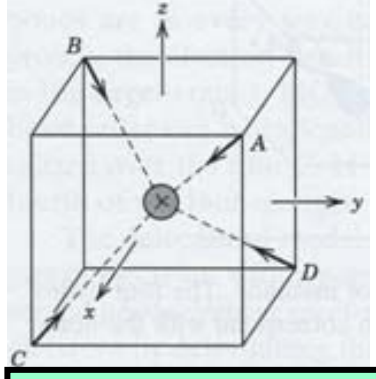



**Figure 4.15** Vector basis for a representation of hydrogen SALCs of $CH_4$.

These are taken as the basis for a representation in $T_d$ to determine the symmetries of hydrogen SALCs.

# 4.3 Localized and Delocalized Molecular Orbitals

From a consideration of shifted and nonshifted vectors, the following reducible representation emerges.




| $T_d$ | $E$ | $8C_3$ | $3C_2$ | $6S_4$ | $6\sigma_d$ |
|---|---|---|---|---|---|
| $\Gamma_{SALC}$ | 4 | 1 | 0 | 0 | 2 |

It decomposes as $\Gamma_{SALC} = A_1 + T_2$.

This means that we can form one totally symmetric SALC and a set of three degenerate SALCs.

The totally symmetric SALC is formed by taking all four hydrogen *1s* wave functions in a positive sense. The normalized $A_1$ SALC can be written as

$$\Phi_1 = \frac{1}{2}\{1s_A + 1s_B + 1s_C + 1s_D\} \qquad (4.21a)$$

# 4.3 Localized and Delocalized Molecular Orbitals

The three degenerate SALCs of $T_2$ are constructed by taking all possible combinations of two hydrogen wave functions in a positive sense with two in a negative sense. The normalized $A_1$ SALC can be written as

$$\Phi_2 = \frac{1}{2}\{1s_A + 1s_B - 1s_C - 1s_D\} \quad (4.21b)$$

$$\Phi_3 = \frac{1}{2}\{1s_A - 1s_B - 1s_C + 1s_D\} \quad (4.21c)$$

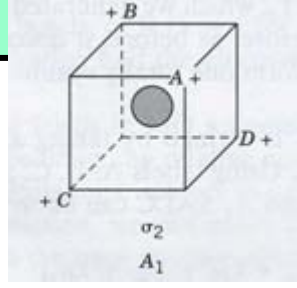
$$\Phi_4 = \frac{1}{2}\{1s_A - 1s_B + 1s_C - 1s_D\} \quad (4.21d)$$

**On carbon**, both the *1s* and *2s* orbitals have $A_1$ symmetry. We assume that the*1s* orbital is a nonbonding.

The *2s* orbital will form bonding and antibonding MOs with the $A_1$ SALC $\Phi_1$. the resulting LCAO-MOs have the forms

$$\sigma_2 = c_1(2s) + c_2\Phi_1 \quad (4.22a)$$

$$\sigma_6^* = c_3(2s) - c_4\Phi_1 \quad (4.22b)$$



# 4.3 Localized and Delocalized Molecular Orbitals

The three *2p* orbitals have $T_2$ symmetry and will form bonding and antibonding combinations with degenerate SALCs $\Phi_2$, $\Phi_3$, and $\Phi_4$.

With each SALC, the bonding LCAO is formed by matching a *2p* orbital whose positive lobe is directed between two hydrogen wave functions with positive sign, and whose negative lobe is directed between two hydrogen wave functions with negative sign.

The resulting wave functions for bonding and antibonding MOs are

$$\sigma_3 = c_5(2p_z) + c_6\Phi_2$$

$$\sigma_7^* = c_7(2p_z) - c_8\Phi_2$$

$$\sigma_4 = c_9(2p_y) + c_{10}\Phi_3$$

$$\sigma_8^* = c_{11}(2p_y) - c_{12}\Phi_3$$

$$\sigma_5 = c_{13}(2p_x) + c_{14}\Phi_4$$

$$\sigma_9^* = c_{15}(2p_x) - c_{16}\Phi_4$$

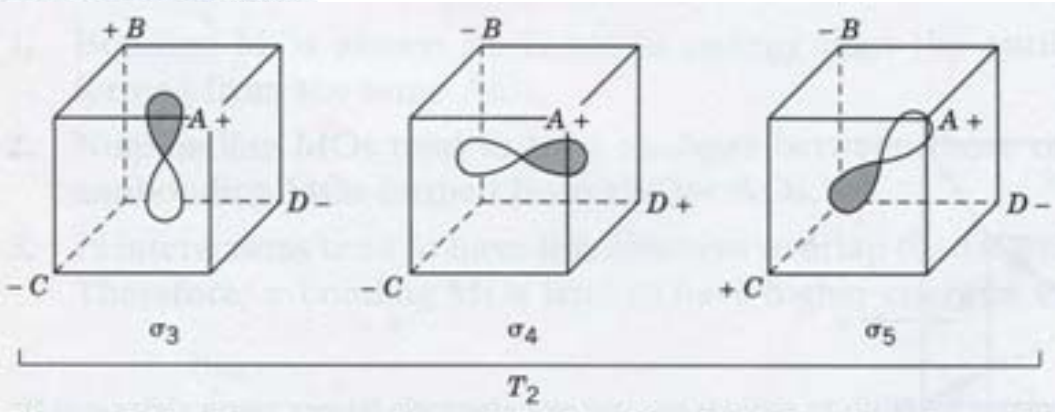



**Figure 4.16** Representations of the bonding LCAOs of methane. The four hydrogen atom wave functions are labeled A, B, C, and D to correspond with the notation of Eqs. (4.21a)–(4.21d).

# 4.3 Localized and Delocalized Molecular Orbitals

Bonding MOs $\sigma_3$, $\sigma_4$, and $\sigma_5$ are degenerate and have the same energy.

Instead of four equal-energy electron pairs confined to four equivalent bonds, we see three pairs of electrons at one energy level and a single pair at a lower energy level.

By the delocalized MO approach, the electron density of each C-H single bond is 75% from electrons in the degenerate $t_2$ Mos and 25% fro electrons in the $a_1$ MO.

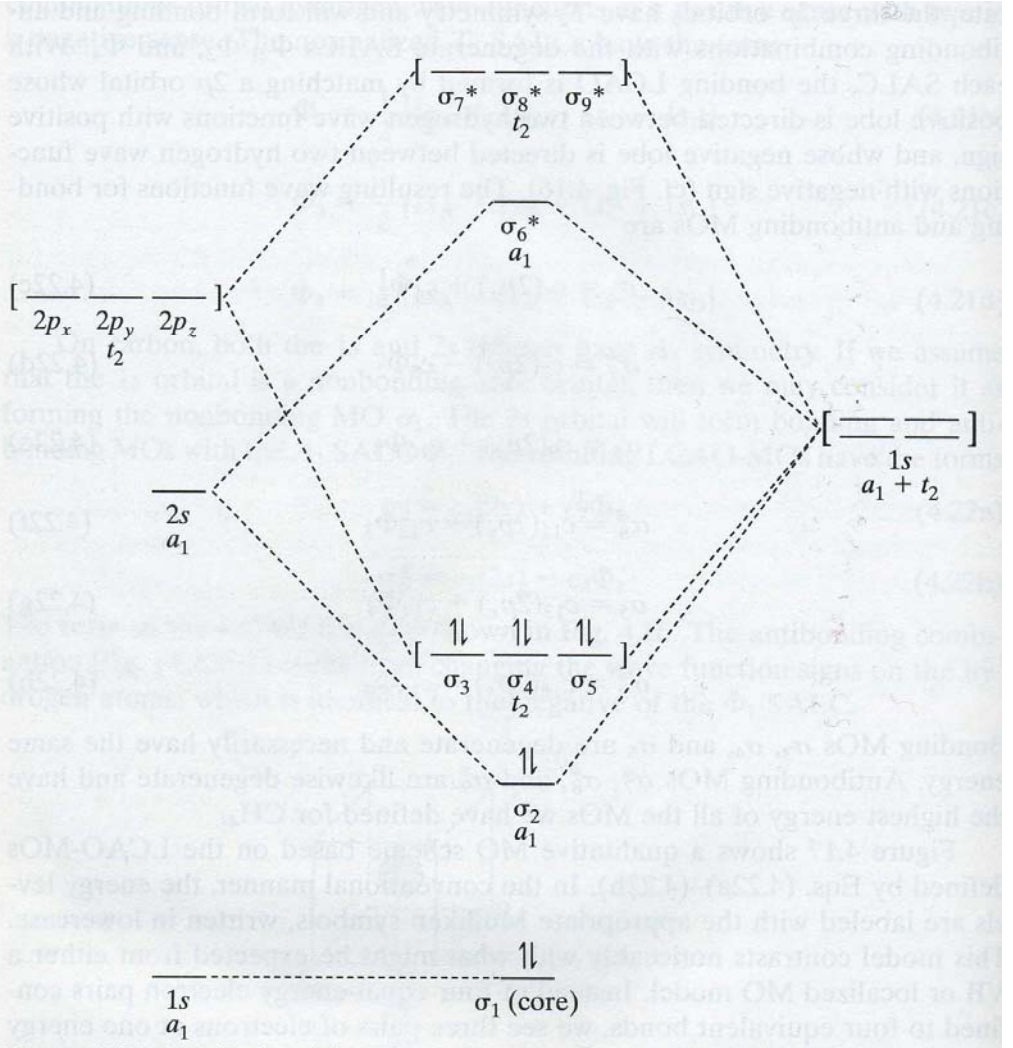



**Figure 4.17** Qualitative delocalized MO energy level scheme for $CH_4$.

# 4.3 Localized and Delocalized Molecular Orbitals

There are two different energies of electrons with a population ratio 3:1.

This is consistent with the observed photoelectron spectrum, which measures ionization energies of valence electrons by determining their kinetic energies after ejection by incident X-ray or UV radiation.

The higher the ionization energy, the lower in energy lies the MO from which the electrons were ejected.

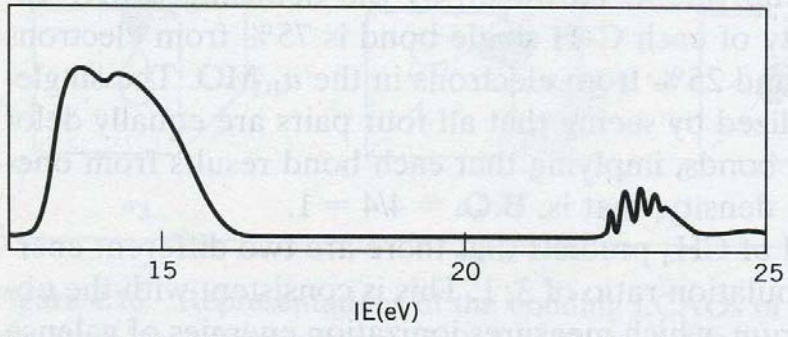



**Figure 4.18** Photoelectron spectrum of $CH_4$. [Adapted with permission of the Royal Society of Chemistry from A. W. Potts, T. A. Williams, and W. C. Price, *Faraday Disc. Chem. Soc.*, **1972**, *54*, 104.]

# 4.3 Localized and Delocalized Molecular Orbitals

Since the highest-dimension irreducible representations of $T_d$ are triply degenerate, there can be no higher than threefold degeneracy among the MOs.

In order words, the fourfold degeneracy among electron pairs that VB and localized MO models suggest is not allowed by the symmetry of the molecule.

Therefore, while all models give comparable qualitative results for bond types and strengths, the delocalized approach generally gives more satisfactory predictions of electron energy levels, consistent with the molecular symmetry.

# 4.4 $MX_n$ molecules with Pi-bonding

If the pendant atoms are members of the second or higher periods of the periodic table, pi interactions with the *p* orbitals on the central atom may be possible.

As predicted VSEPR theory, carbon dioxide is a linear molecule ($D_{\infty h}$).

In the VB model, the carbon atom is assumed to have *sp* hybrid orbitals, each with two electrons, which form separate sigma bonds by overlap and electron-pair sharing with a $2p_z$ orbital on each oxygen.

This leaves empty $2p_x$ and $2p_y$ orbitals on the carbon atom, which can form pi bonds by overlap with a $2p_x$ orbital on one oxygen atom and a $2p_y$ orbital on the other oxygen atom.

# 4.4 $MX_n$ molecules with Pi-bonding

This simplistic model predicts two equivalent C=O double bonds ($\sigma$ + $\pi$), with the maximum C-$O_a$ pi overlap in the xy plane and the maximum C-$O_b$ pi overlap in the yz plane.

A localized MO model follows directly from this VB model. Pairs of equivalent sigma-bonding MOs would be lie lowest energy, with pairs of equivalent pi-bonding MOs lying somewhat higher in energy.

The highest-energy occupied MOs would be the nonbonding 2*s* and *2p* orbitals localized on the oxygen atoms

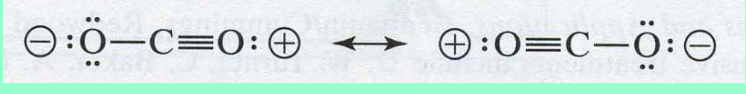
The electronic configuration for this localized MO model is

$$[(\sigma_a)^2(\sigma_b)^2][(\pi_a)^2(\pi_b)^2][(\sigma_a^n)^2(\sigma_b^n)^2][(\pi_a^n)^2(\pi_b^n)^2]$$

# 4.4 $MX_n$ molecules with Pi-bonding

On the basis of either the VB or localized MO models, we might expect each bond to have the typical C=O bond length of 124 pm. Instead, the observed length is 116pm, suggesting a somewhat stronger bond.

This is somewhat rationalized by admitting the following resonance forms.



We can anticipate, then, that a general MO approach, which inherently assumes delocalization, might yield a more satisfying model.

# 4.4 $MX_n$ molecules with Pi-bonding

In setting up a general MO treatment, we will assume initially that the oxygen 2*s* electrons do not participate in bond formation, as we did with the VB and localized MO approaches.

Having for the moment ruled out interactions with carbon AOs, we can assume that the two SALCs that can be defined for these orbitals will be equivalent to two nonbonding $\sigma^n$ MOs, whose forms are

$$\sigma_g^n(O_{2s}) = \frac{1}{\sqrt{2}}(2s_a + 2s_b) \qquad (4.24a)$$

$$\sigma_u^n(O_{2s}) = \frac{1}{\sqrt{2}}(2s_a - 2s_b) \qquad (4.24b)$$

These belong to the species $\Sigma_g^+$ and $\Sigma_u^+$ respectively, in $D_{\infty h}$. They are identical in form to the hydrogen SALCs of $BeH_2$.

# 4.4 $MX_n$ molecules with Pi-bonding

Forming SALCs among the 2p orbitals on the two oxygen atoms.

These will form MOs by combination with the 2s and 2p orbitals on the central carbon atom.

A set of six vectors, which we will take as the basis for a representation for oxygen SALCs.

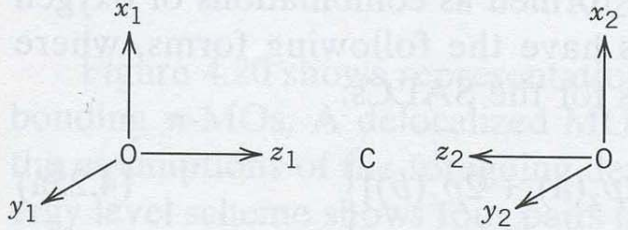



**Figure 4.19** Vector basis for a representation of oxygen SALCs of $CO_2$.

We will generate the representation in the subgroup $D_{2h}$ employing the correlation technique.

# 4.4 $MX_n$ molecules with Pi-bonding

We obtain the following reducible representation.

In the case of $C_2(z)$, the operation shifts the two x vectors and the two y vectors into negatives of themselves, contributing -4 to the overall character. The two z vectors, however, are not shifted and contribute +2 to the overall character.

| $D_{2h}$ | $E$ | $C_2(z)$ | $C_2(y)$ | $C_2(x)$ | $i$ | $\sigma(xy)$ | $\sigma(xz)$ | $\sigma(yz)$ |
|---|---|---|---|---|---|---|---|---|
| $\Gamma_{SALC}$ | 6 | −2 | 0 | 0 | 0 | 0 | 2 | 2 |

Using eq (3.1) and tabular method

| $D_{2h}$ | $E$ | $C_2(z)$ | $C_2(y)$ | $C_2(x)$ | $i$ | $\sigma(xy)$ | $\sigma(xz)$ | $\sigma(yz)$ | | |
|---|---|---|---|---|---|---|---|---|---|---|
| $\Gamma_{SALC}$ | 6 | −2 | 0 | 0 | 0 | 0 | 2 | 2 | $\Sigma$ | $\Sigma/8$ |
| $A_g$ | 6 | −2 | 0 | 0 | 0 | 0 | 2 | 2 | 8 | 1 |
| $B_{1g}$ | 6 | −2 | 0 | 0 | 0 | 0 | −2 | −2 | 0 | 0 |
| $B_{2g}$ | 6 | 2 | 0 | 0 | 0 | 0 | 2 | −2 | 8 | 1 |
| $B_{3g}$ | 6 | 2 | 0 | 0 | 0 | 0 | −2 | 2 | 8 | 1 |
| $A_u$ | 6 | −2 | 0 | 0 | 0 | 0 | −2 | −2 | 0 | 0 |
| $B_{1u}$ | 6 | −2 | 0 | 0 | 0 | 0 | 2 | 2 | 8 | 1 |
| $B_{2u}$ | 6 | 2 | 0 | 0 | 0 | 0 | −2 | 2 | 8 | 1 |
| $B_{3u}$ | 6 | 2 | 0 | 0 | 0 | 0 | 2 | −2 | 8 | 1 |

We see that $\Gamma_{SALC} = A_g + B_{2g} + B_{3g} + B_{1u} + B_{2u} + B_{3u}$ *in* $D_{2h}$.

# 4.4 $MX_n$ molecules with Pi-bonding

We see that $\Gamma_{SALC} = A_g + B_{2g} + B_{3g} + B_{1u} + B_{2u} + B_{3u}$ *in* $D_{2h}$.

We can correlate these species with the equivalent species in $D_{\infty h}$ by using table 3.9.

$\Gamma_{SALC} = \Sigma_g^+ + \Pi_g + \Sigma_u^+ + \Pi_u$.

This means that our six SALCs will be composed of two nondegernerate and two of doubly degenerate.

We must find the **AOs on the central carbon atom that have the appropriate symmetry** to from bonding and antibonding combinations with these SALCs.

From character table of $D_{\infty h}$, the 2s orbital transforms as $\Sigma_g^+$, the $2p_z$ orbital transforms as $\Sigma_u^+$, and the $2p_x$ and $2p_y$ orbitals transform degenerately as $\Pi_u$.

# 4.4 $MX_n$ molecules with Pi-bonding

We now ready to combine AOs and SALCs.

The 2s and $2p_z$ orbitals will have sigma interactions with the pendant atom SALCs of $\Sigma_g^+$ and $\Sigma_u^+$ symmetry, respectively.

The degenerate $2p_x$ and $2p_y$ orbitals on carbon interact with SALCs of $\Pi_u$.

A degenerate pair of SALCs of $\Pi_g$ symmetry for which there are no matching AOs. They form two nonbonding $\pi^n$-MOs.

# 4.4 $MX_n$ molecules with Pi-bonding

There are four bonds, just as the VB and localized MO models predict, but now the electrons are seen to be evenly distributed across the molecule.

The delocalization of the pi-bonding system gives extra strength to the C-O bonds in $CO_2$, resulting in somewhat shorter C-O bond length.

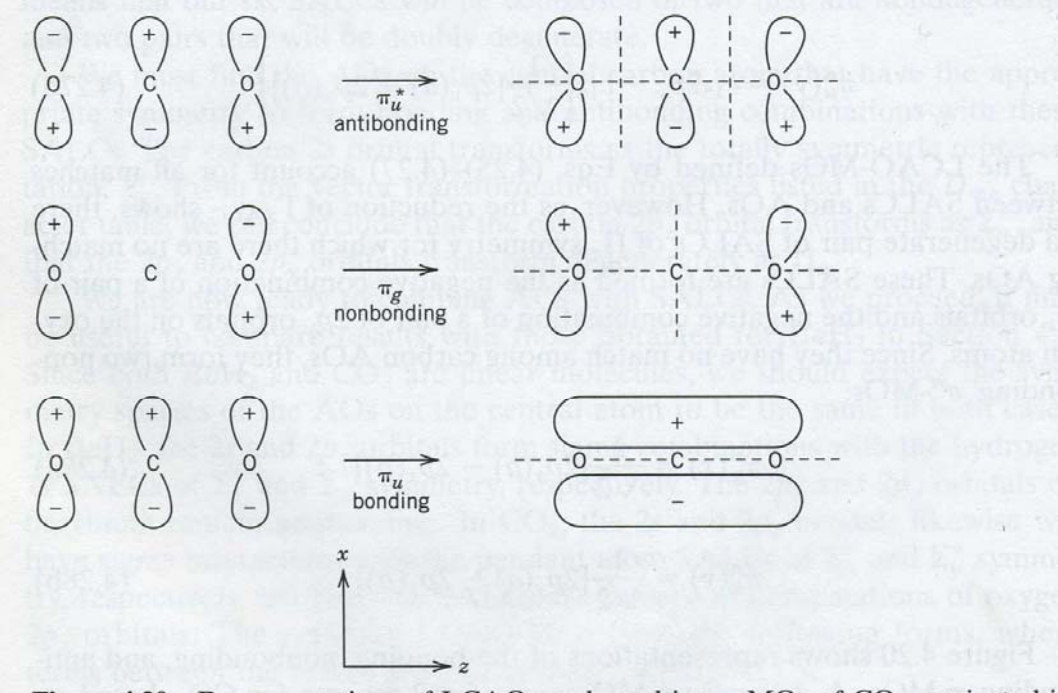



**Figure 4.20** Representations of LCAOs and resulting $\pi$-MOs of $CO_2$, projected i the $xz$ plane. Nodal planes perpendicular to the page are shown with dashed lines. Degenerate LCAOs and MOs similar to those shown lie in the $yz$ plane.

# 4.4 $MX_n$ mole

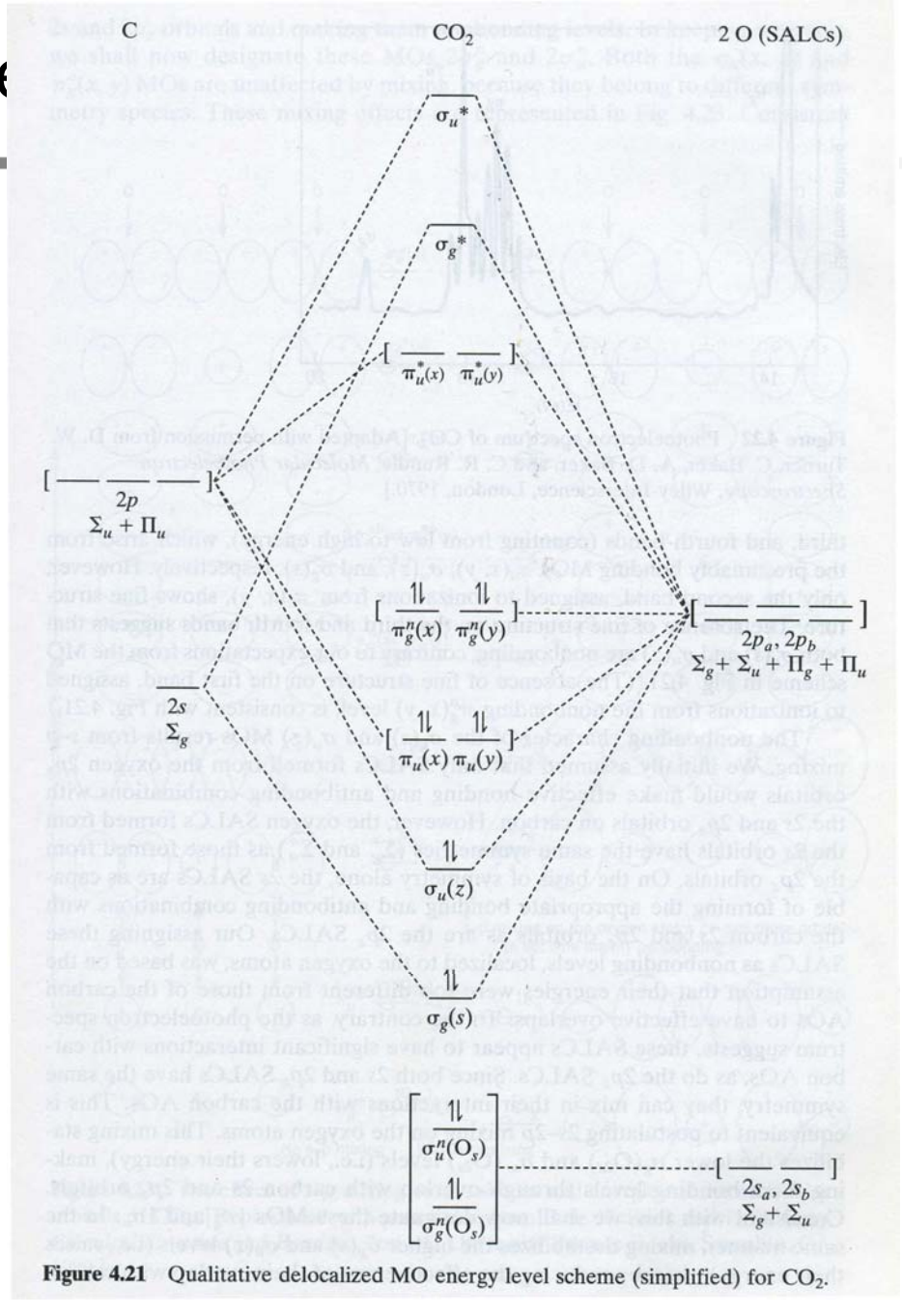



**Figure 4.21** Qualitative delocalized MO energy level scheme (simplified) for $CO_2$.

# 4.4 $MX_n$ molecules with Pi-bonding

The electronic configuration

$$[\sigma_g^n]^2[\sigma_u^n]^2[\sigma_g(s)]^2[\sigma_u(z)]^2\{[\pi_u(x)]^2[\pi_u(y)]^2\}\{[\pi_g^n(x)]^2[\pi_g^n(y)]^2\}$$

$$(\sigma_g^n)^2(\sigma_u^n)^2[\sigma_g(s)]^2[\sigma_u(z)]^2[\pi_u(x,\,y)]^4[\pi_g^n(x,\,y)]^4.$$

The electronic configuration for localized MO medel

$$[(\sigma_a)^2(\sigma_b)^2][(\pi_a)^2(\pi_b)^2][(\sigma_a^n)^2(\sigma_b^n)^2][(\pi_a^n)^2(\pi_b^n)^2]$$

From this we should expect the photoelectron spectrum to exhibit six bands, resulting from ionizations from each of the levels.

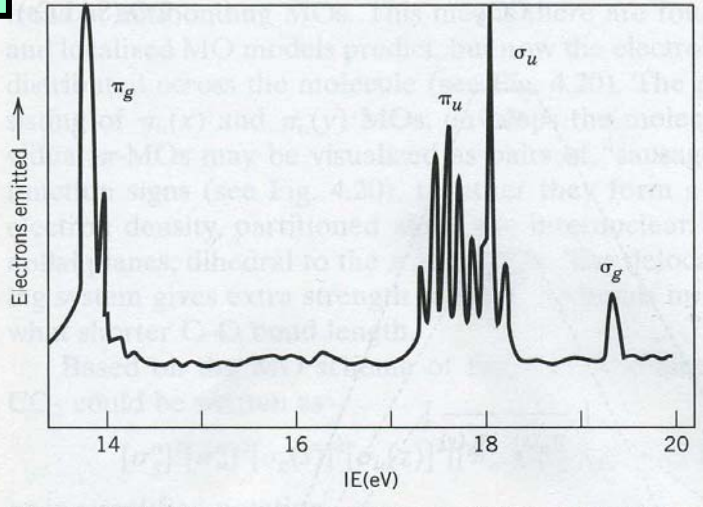



**Figure 4.22** Photoelectron spectrum of $CO_2$. [Adapted with permission from D. W. Turner, C. Baker, A. D. Baker, and C. R. Rundle, *Molecular Photoelectron Spectroscopy*, Wiley-Interscience, London, 1970.]

# 4.4 $MX_n$ molecules with Pi-bonding

If our MO predictions are entirely correct, we also should expect vibrational fine structure on the second, third, and fourth bands.

However, only the second band shows fine structure.

The absence of fine structure on the third and fourth bands suggests that both are nonbonding, contrary to our expectations from the MO scheme.

The nonbonding character of the $\sigma_g(s)$ and $\sigma_u(z)$ MOs results from s-p mixing. We initially assumed that only SALCs formed from the oxygen $2p_z$ orbitals would make effective bonding and antibonding combinations with 2s and $2p_z$ orbitals on carbon.

However, the oxygen SALCs formed from the 2s orbitals have the same symmetries ($\Sigma_g$ and $\Sigma_u$) as those formed from the $2p_z$ orbitals.

# 4.4 $MX_n$ molecules with Pi-bonding

Our assigning these SALCs as nonbonding levels, localized to the oxygen atoms, was based on the assumption that their energies were too different from those of the carbon AOs to have effective overlaps.

Since both 2s and $2p_z$ SALCs have the same symmetry, they can mix in their interactions with the carbon AOs.

# 4.4 $MX_n$

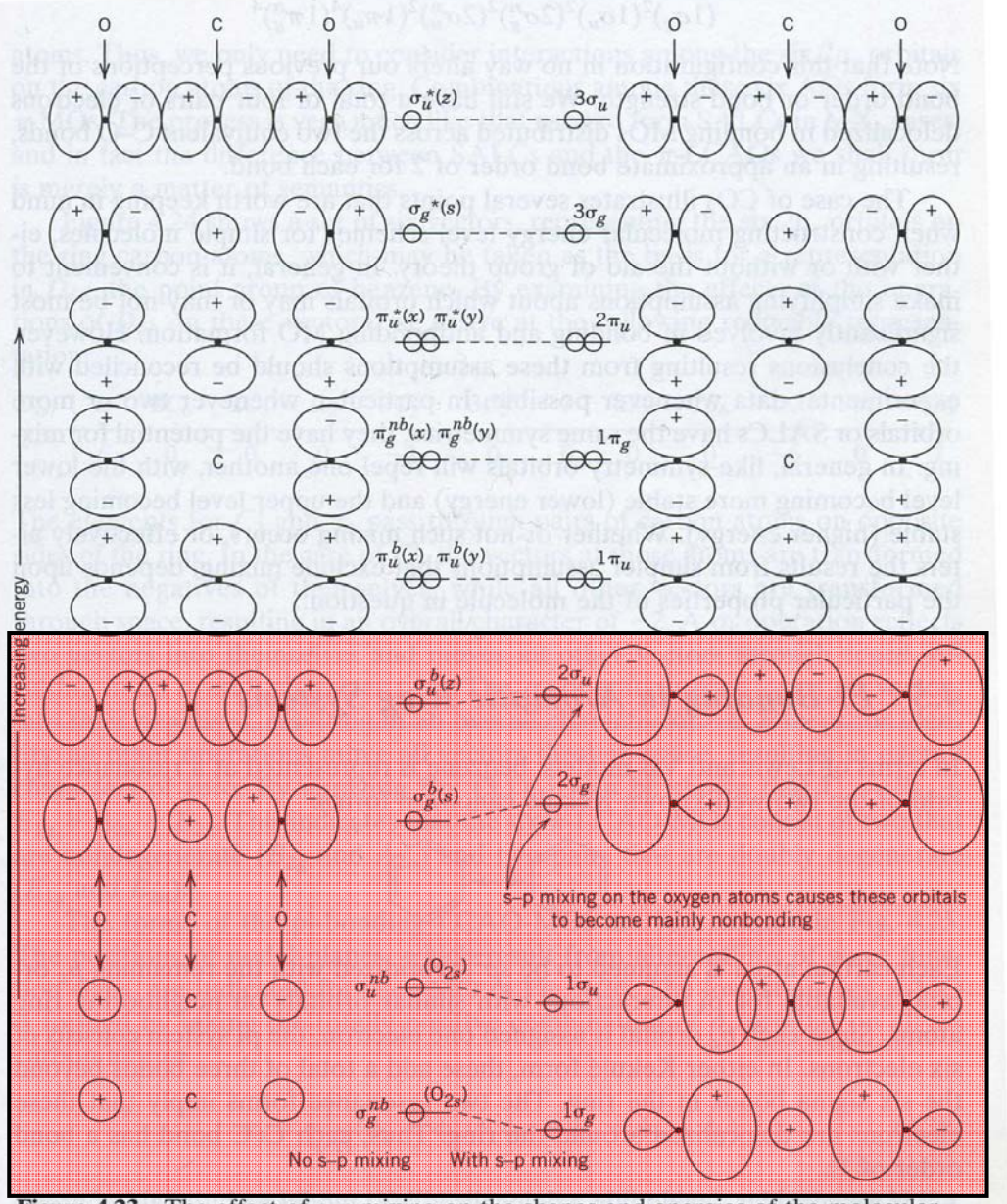
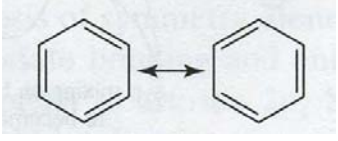



**Figure 4.23** The effect of *s–p* mixing on the shapes and energies of the molecular orbitals of $CO_2$. [Reproduced with permission from R. L. DeKock and H. B. Gray, *Chemical Structure and Bonding*, 2nd ed., University Science Books, Sausalito, CA, 1989.]

# 4.5 Pi-Bonding in Aromatic Ring System

In terms of Lewis and VB models, benzene is represented as a resonance hybrid.



Each carbon atom is assumed to be $sp^2$-hybridized with the remaining $p_z$ orbital available for pi-interactions with similar orbitals on neighboring ring atoms.

Benzene has no central atom whose orbitals are to be matched with SALCs formed from combinations of orbitals on outer-lying atoms. Thus, we only need to consider interactions among the six $2p_z$ orbitals on the carbon atoms of the ring.

# 4.5 Pi-Bonding in Aromatic Ring System

A set of six vectors, representing the six $2p_z$ orbitals on the carbon atoms, which may be taken as the basis for a representation in $D_{6h}$, the point group of benzene.

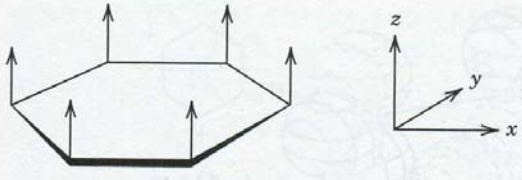



**Figure 4.24** Vector basis for a representation of $\pi$-MOs of benzene.

Reducible representation

| $D_{6h}$ | $E$ | $2C_6$ | $2C_3$ | $C_2$ | $3C_2'$ | $3C_2''$ | $i$ | $2S_3$ | $2S_6$ | $\sigma_h$ | $3\sigma_d$ | $3\sigma_v$ |
|---|---|---|---|---|---|---|---|---|---|---|---|---|
| $\Gamma_\pi$ | 6 | 0 | 0 | 0 | −2 | 0 | 0 | 0 | 0 | −6 | 0 | 2 |

We can obtain that $\Gamma_\pi = B_{2g} + E_{1g} + A_{2u} + E_{2u}$

# Aromatic Ring System

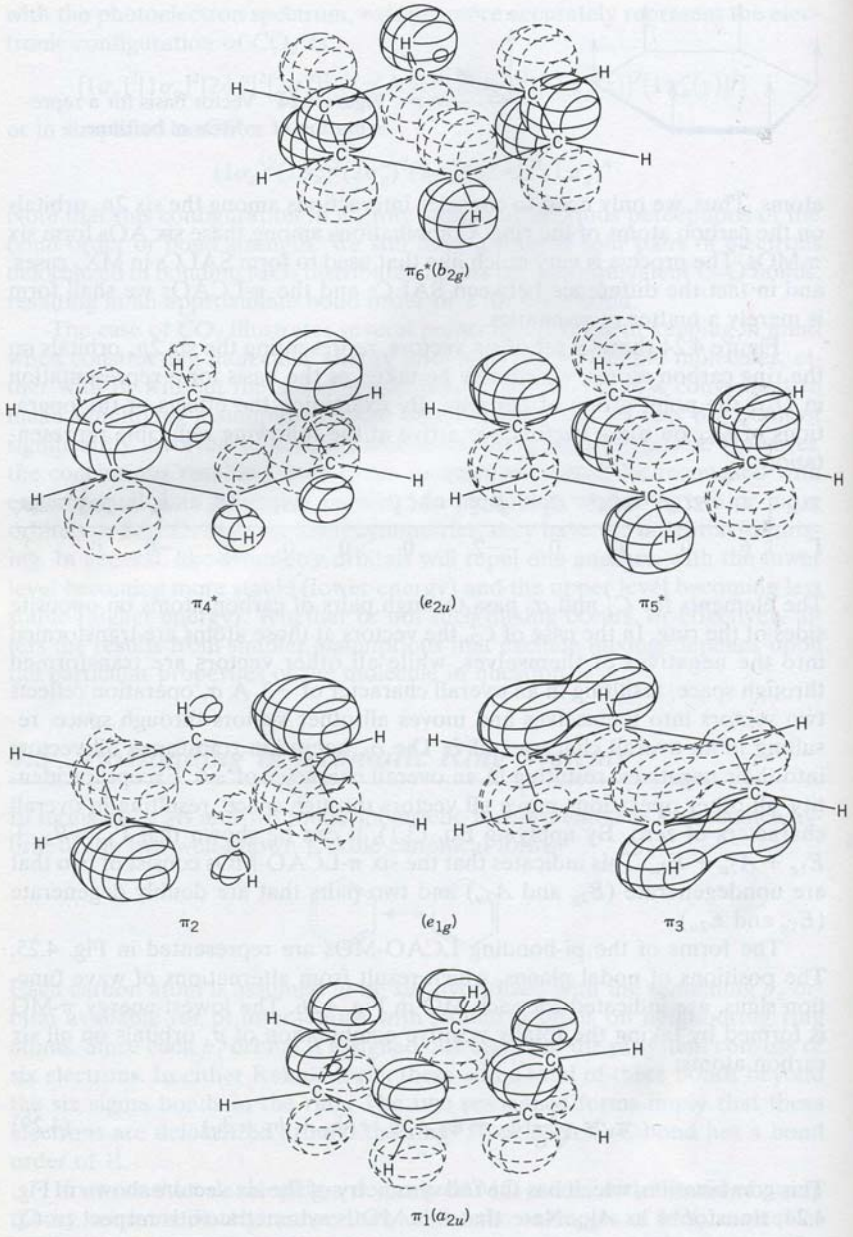



**Figure 4.25** Delocalized $\pi$-MOs of benzene. Solid and dotted line contours represent positive and negative signs of the wave function, respectively. [Reproduced with permission from William L. Jorgensen and Lionel Salem, *The Organic Chemist's Book of Orbitals*, Academic Press, New York, 1973.]

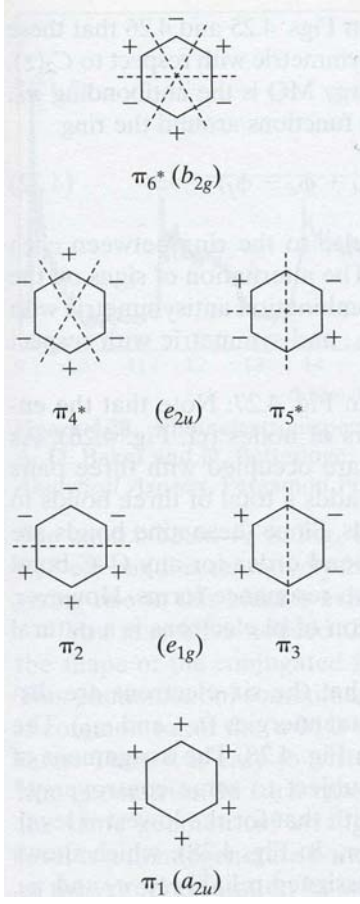



**Figure 4.26** Nodal planes (perpendicular to the ring plane) for the pi-bonding and antibonding MOs of benzene.

# 4.5 Pi-Bonding in Aromatic Ring System

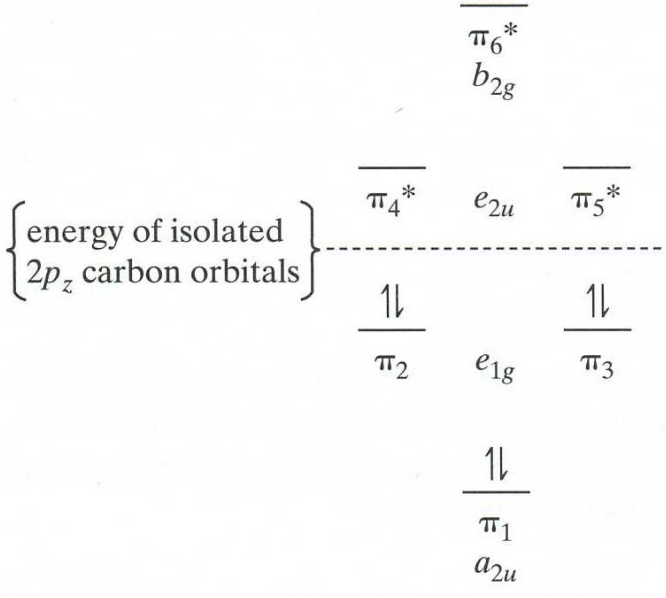



**Figure 4.27** The $\pi$-MO energy level scheme for benzene.

The pattern of the levels mimics the shape of the conjugated ring system.

# 4.5 Pi-Bonding in Aromatic Ring System

The π–MO scheme for benzene suggests that the six electrons are distributed in a 1:2 ratio between two distinct orbital energies.

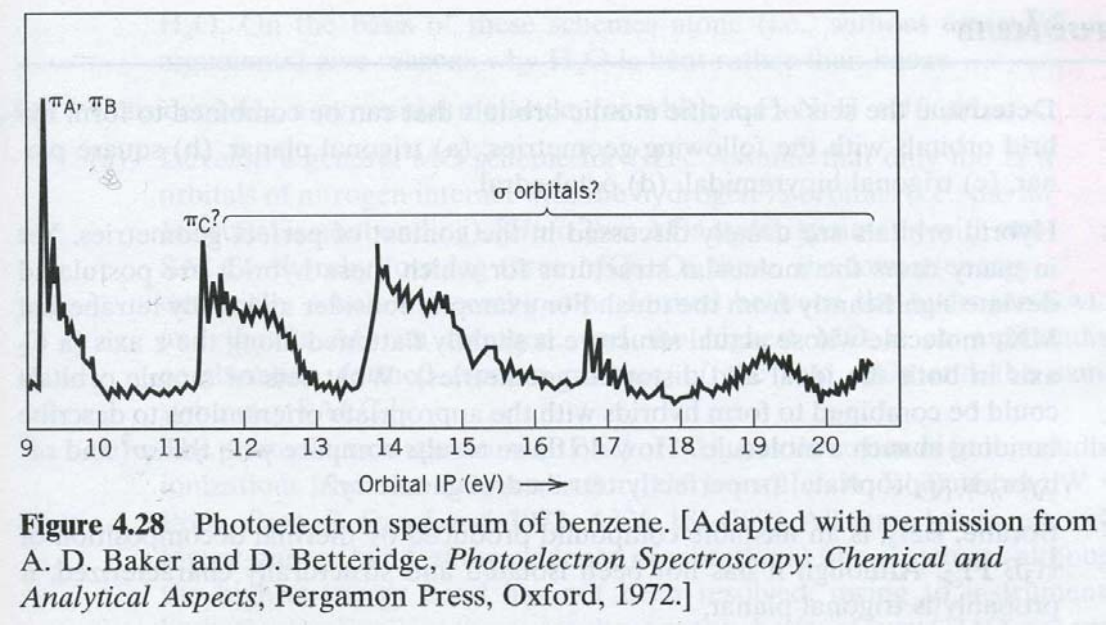



**Figure 4.28** Photoelectron spectrum of benzene. [Adapted with permission from A. D. Baker and D. Betteridge, *Photoelectron Spectroscopy: Chemical and Analytical Aspects*, Pergamon Press, Oxford, 1972.]